Higher-order anisotropic flows and dihadron correlations in Pb-Pb collisions at $\sqrt{s_{NN}} = 2.76$ TeV in a multiphase transport model

Jun Xu[1, *] and Che Ming Ko[2, †]

[1]*Cyclotron Institute, Texas A&M University, College Station, Texas 77843-3366, USA*
[2]*Cyclotron Institute and Department of Physics and Astronomy,*
Texas A&M University, College Station, Texas 77843-3366, USA
(Dated: September 28, 2011)

Using a multiphase transport model that includes both initial partonic and final hadronic scatterings, we have studied higher-order anisotropic flows as well as dihadron correlations as functions of pseudorapidity and azimuthal angular differences between trigger and associated particles in Pb-Pb collisions at $\sqrt{s_{NN}} = 2.76$ TeV. With parameters in the model determined previously from fitting the measured multiplicity density of mid-pseudorapidity charged particles in central collisions and their elliptic flow in mid-central collisions, the calculated higher-order anisotropic flows from the two-particle cumulant method reproduce approximately those measured by the ALICE Collaboration, except at small centralities where they are slightly overestimated. Similar to experimental results, the two-dimensional dihadron correlations at most central collisions show a ridge structure at the near side and a broad structure at the away side. The short- and long-range dihadron azimuthal correlations, corresponding to small and large pseudorapidity differences, respectively, are studied for triggering particles with different transverse momenta and are found to be qualitatively consistent with experimental results from the CMS Collaboration. The relation between the short-range and long-range dihadron correlations with that induced by back-to-back jet pairs produced from initial hard collisions is also discussed.

PACS numbers: 25.75.-q, 12.38.Mh, 24.10.Lx

I. INTRODUCTION

Heavy ion collisions at the Relativistic Heavy-Ion Collider (RHIC) have made it possible to obtain important information on the properties of the quark-gluon plasma (QGP) that is produced in these collisions [1–4]. Among the many observables that have been used to infer the properties of the QGP are the anisotropic flows of produced particles, particularly the elliptic flow (v_2) [5] that corresponds to the second-order harmonic coefficient of the anisotropic flow and is appreciable in noncentral collisions of identical nuclei. More recently, it was found that the triangular flow v_3 that corresponds to the third-order harmonic coefficient of the anisotropic flow could also be significant in collisions of all centralities as a result of initial density fluctuations in the collision geometry [6, 7]. Furthermore, it was shown that studying v_3 together with v_2 can help better constrain the properties of the QGP [8, 9]. Also, it was suggested that useful information about the QGP could be obtained from the dihadron correlation [10] between lower-p_T associated particles from the medium response to the away-side jet and higher-p_T trigger particles produced from the near-side jet. Studies based on the transport model showed that higher-order anisotropic flows, especially the triangular flow, had a large effect on dihadron correlations induced by initial energetic jets [11, 12]. To extract

from the dihadron correlation information on the interactions of energetic jets produced from initial hard collisions with medium partons in the quark-gluon plasma requires, however, the subtraction of the background contribution from anisotropic flows and their fluctuations, and this is a topic of great current interest [6, 11–14].

Recently, results from the first Pb-Pb collisions at $\sqrt{s_{NN}} = 2.76$ TeV at the Large Hadron Collider (LHC) have attracted a lot of attentions [15–18]. In the most central collisions ($0 - 5\%$), the multiplicity density of produced charged particles at mid-pseudorapidity is 2.2 times of that in Au+Au collisions at $\sqrt{s_{NN}} = 200$ GeV at RHIC. The measured elliptic flow, which can provide more reliable information about the produced QGP [19], is of a similar magnitude as that measured at RHIC. Besides, experimental data on higher-order flows [20] and dihadron correlations [21] have also become available, providing the opportunity to study the properties of the hotter and denser QGP formed at LHC. In particular, it was found that the long-range dihadron azimuthal correlations could be entirely accounted for by the anisotropic flows [20, 21].

In a recent work [22], we studied Pb-Pb collisions at $\sqrt{s_{NN}} = 2.76$ TeV in a multiphase transport (AMPT) model. The AMPT model is a hybrid model with the initial particle distribution generated by the heavy ion jet interaction generator (HIJING) model [23]. In the version of string melting, which was used in the previous work [22] and will be used in the present study, all hadrons produced in the HIJING model through Lund string fragmentation are converted to their valence quarks and antiquarks, whose evolution in time and space

*Electronic address: xujun@comp.tamu.edu
†Electronic address: ko@comp.tamu.edu

is modeled by Zhang's parton cascade (ZPC) model [24]. After their scatterings, quarks and aniquarks are converted via a spatial coalescence model to hadrons, and the scatterings among them are described by a relativistic transport (ART) model [25]. For a recent review of the AMPT model, we refer the readers to Ref. [26]. By adjusting the values of parameters in the Lund string fragmentation function and the parton scattering cross section, we fitted the differential elliptic flow at $40-50\%$ centrality window and reproduced reasonably well the centrality dependence of both the multiplicity density and the elliptic flow of mid-pseudorapidity charged particles [22], although the transverse momentum spectrum at most central collisions is softer than the data from the ALICE Collaboration as a result of the use of massless partons in the model that are less affected by the radial flow [26]. In the present paper, we study higher-order anisotropic flows and dihadron correlations in Pb-Pb collisions at LHC by using the AMPT model with the newly fitted parameters. Our results show that in heavy ion collisions at LHC higher-order flows are appreciable and a ridge structure exists in the dihadron correlation as seen in the experiments [21]. The ridge structure is a result of the longitudinal expansion of the anisotropic flows as pointed out previously in Ref. [27].

This paper is organized as follows. We first give some general discussions on anisotropic flows and dihadron correlations in Sec. II. We then show in Sec. III A the results on the centrality dependence of anisotropic flows and their transverse momentum dependence in most central and mid-central collisions and in Sec. III B those on the dihadron correlations in most central collisions. A summary is then given in Sec. IV.

II. ANISOTROPIC FLOWS AND DIHADRON CORRELATIONS

To help understand the results of anisotropic flows and dihadron correlations in the following sections, we first discuss generally the contribution from anisotropic flows and their fluctuations as well as the nonflow contribution to the two-dimensional dihadron correlation between two particles.

The momentum distribution of produced particles in a heavy ion collision event can be generally written as

$$f(p_T, \phi, \eta) = \frac{N(p_T, \eta)}{2\pi} \left\{ 1 + 2\sum_n v_n(p_T, \eta) \cos[n(\phi - \Psi_n)] \right\}$$
(1)

where ϕ is the azimuthal angle, Ψ_n is the nth-order event plane angle, and $N(p_T, \eta)$ and $v_n(p_T, \eta)$ are the number of particles of transverse momentum p_T and pseudorapidity η and their nth-order anisotropic flows, respectively. The correlation between two particles with transverse momenta p_T^a and p_T^b and azimuthal angular difference $\Delta\phi$ and pseudorapidity difference $\Delta\eta$ within the same event can be calculated from Eq. (1) by using

the orthonormal relation of the harmonic terms, i.e.,

$$\frac{d^2 N_{\text{pair}}^{\text{same}}}{d\Delta\eta d\Delta\phi} = \frac{1}{\eta_{\max} - \eta_{\min}} \int_{\eta_{\min}}^{\eta_{\max}} d\eta$$
$$\times \frac{1}{2\pi} \int_0^{2\pi} d\phi f(p_T^a, \phi, \eta) f(p_T^b, \phi + \Delta\phi, \eta + \Delta\eta)$$
$$= \frac{1}{\eta_{\max} - \eta_{\min}} \int_{\eta_{\min}}^{\eta_{\max}} d\eta \frac{N(p_T^a, \eta) N(p_T^b, \eta + \Delta\eta)}{(2\pi)^2}$$
$$\times \left[1 + 2\sum_n v_n(p_T^a, \eta) v_n(p_T^b, \eta + \Delta\eta) \cos(n\Delta\phi) \right] .(2)$$

By neglecting the correlation between particle number and flow, the event average of the two-particle correlation can then be approximated by

$$\left\langle \frac{d^2 N_{\text{pair}}^{\text{same}}}{d\Delta\eta d\Delta\phi} \right\rangle_{\text{e}}$$
$$\approx \frac{1}{\eta_{\max} - \eta_{\min}} \int_{\eta_{\min}}^{\eta_{\max}} d\eta \left\langle \frac{N(p_T^a, \eta) N(p_T^b, \eta + \Delta\eta)}{(2\pi)^2} \right\rangle_{\text{e}}$$
$$\times \left[1 + 2\sum_n \langle v_n(p_T^a, \eta) v_n(p_T^b, \eta + \Delta\eta) \rangle_{\text{e}} \cos(n\Delta\phi) \right] .(3)$$

where $\langle \cdots \rangle_{\text{e}}$ denotes average over all events.

Assuming that the dependence of the anisotropic flows on the pseudorapidity is weak, the second term in Eq. (3) can be taken out of the integration and further expressed approximately as

$$\langle v_n(p_T^a, \eta) v_n(p_T^b, \eta + \Delta\eta) \rangle_{\text{e}} \cos(n\Delta\phi)$$
$$\approx \langle v_n(p_T^a) \rangle_{\text{e}} \langle v_n(p_T^b) \rangle_{\text{e}} \cos(n\Delta\phi)$$
$$+ FF(v_n(p_T^a), v_n(p_T^b)) \cos(n\Delta\phi) + NF(\Delta\phi, \Delta\eta),(4)$$

where $FF(v_n(p_T^a), v_n(p_T^b))$ is the flow fluctuation contribution and $NF(\Delta\phi, \Delta\eta)$ is the non-flow contribution due to jet correlations or resonance decays that are important only for small $\Delta\eta$ and $\Delta\phi \sim 0$ or π. For the case of $p_T^a = p_T^b$, the usual anisotropic flows calculated using the two-particle cumulant method [28, 29] after integrating the pseudorapidity difference is then obtained, i.e.,

$$v_n\{2\} = \sqrt{\langle \cos(n\Delta\phi) \rangle}.$$
(5)

Using the fact that the first term in Eq. (3) can be calculated from the mix-event correlation, i.e.,

$$\left\langle \frac{d^2 N_{\text{pair}}^{\text{mix}}}{d\Delta\eta d\Delta\phi} \right\rangle_{\text{e}}$$
$$= \frac{1}{\eta_{\max} - \eta_{\min}} \int_{\eta_{\min}}^{\eta_{\max}} d\eta \left\langle \frac{N(p_T^a, \eta) N(p_T^b, \eta + \Delta\eta)}{(2\pi)^2} \right\rangle_{\text{e}},$$
(6)

since the harmonic terms vanish due to the independent

event plane angles in different events, it follows that

$$\left\langle \frac{d^2 N_{\text{pair}}^{\text{same}}}{d\Delta\eta d\Delta\phi} \right\rangle_{\text{e}} \bigg/ \left\langle \frac{d^2 N_{\text{pair}}^{\text{mix}}}{d\Delta\eta d\Delta\phi} \right\rangle_{\text{e}}$$
$$\approx 1 + \langle v_n(p_T^a) \rangle_e \langle v_n(p_T^b) \rangle_e \cos(n\Delta\phi)$$
$$+ FF(v_n(p_T), v_n(p_T^b)) \cos(n\Delta\phi) + NF(\Delta\phi, \Delta\eta). \quad (7)$$

The dihadron correlations thus have contributions from anisotropic flows and their fluctuations as well as the nonflow contribution.
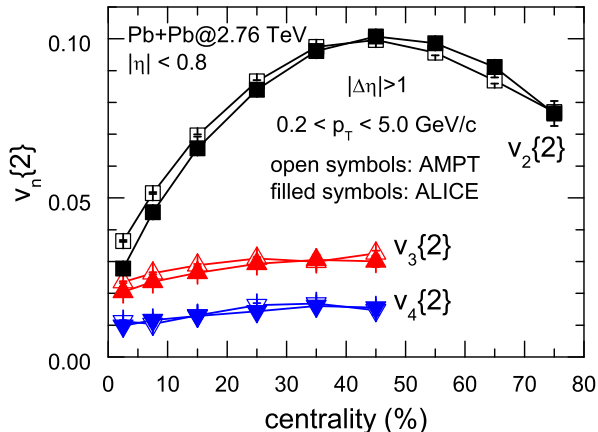
III. RESULTS

A. Anisotropic flows

FIG. 1: (Color online) Centrality dependence of $v_n(n = 2, 3, 4)$ for mid-pseudorapidity ($|\eta| < 0.8$) charged particles obtained from the two-particle cumulant method in Pb-Pb collisions at $\sqrt{s_{NN}} = 2.76$ TeV from the string melting AMPT model. The ALICE data (filled symbols) are taken from Ref. [20].

We first consider the centrality dependence of anisotropic flows $v_n(n = 2, 3, 4)$ for mid-pseudorapidity charged particles in Pb-Pb collisions at $\sqrt{s_{NN}} = 2.76$ TeV from the string melting AMPT model using the two-particle cumulant method (Eq. (5)). To reduce nonflow effects on the calculated v_n, only pairs with pseudorapidity difference $|\Delta\eta| > 1$ are considered in the present study as in experimental analyses [20] . Results for transverse-momentum-integrated ($0.2 < p_T < 5.0$ GeV/c) anisotropic flows are shown by open symbols in Fig. 1. Compared with the ALICE data (filled symbols) [20], the AMPT model reproduces reasonably well the centrality dependence of $v_n(n = 2, 3, 4)$ except that

they are slightly larger at small centralities. This is due to the fact that we have chosen in our previous work [22] to fit the elliptic flow at the $40 - 50\%$ centrality window.
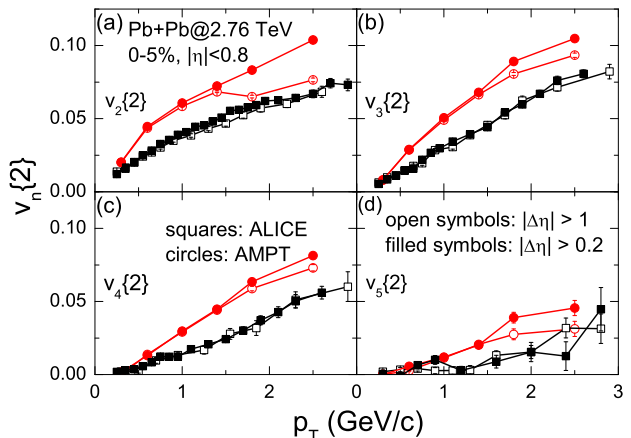

FIG. 2: (Color online) Transverse momentum dependence of v_2 (a), v_3 (b), v_4 (c), and v_5 (d) for mid-pseudorapidity ($|\eta| < 0.8$) charged particles obtained from the two-particle cumulant method in most central ($0 - 5\%$) Pb-Pb collisions at $\sqrt{s_{NN}} = 2.76$ TeV from the string melting AMPT model. The ALICE data (squares) are taken from Ref. [20]. Results for $|\Delta\eta| > 0.2$ and $|\Delta\eta| > 1$ are shown by filled and open symbols, respectively.
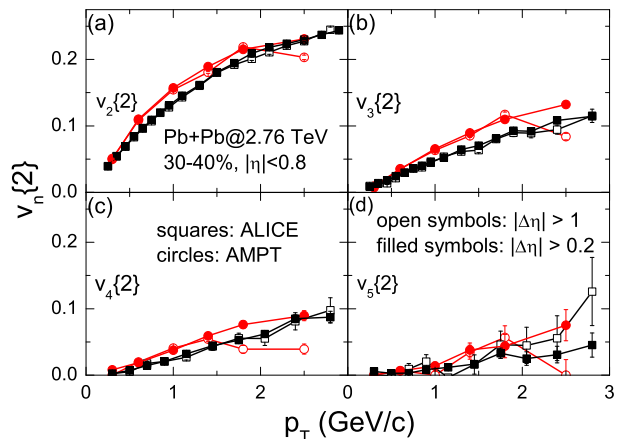

FIG. 3: (Color online) Same as Fig. 2 but for centrality $30 - 40\%$.

In Figs. 2 and 3, we display by circles the transverse momentum dependence of anisotropic flows $v_n(n = 2, 3, 4, 5)$ of mid-pseudorapidity ($|\eta| < 0.8$) charged particles in the most central ($0 - 5\%$) and the mid-central ($30 - 40\%$) Pb-Pb collisions at $\sqrt{s_{NN}} = 2.76$ TeV, re-

spectively, from the AMPT model with string melting, and compare them with the ALICE data (squares) from Ref. [20]. It is seen that the anisotropic flows for different pseudorapidity cut $|\Delta\eta| > 0.2$ and $|\Delta\eta| > 1$ are similar to those from the ALICE data, while at larger transverse momenta in the case of the smaller pseudorapdity cut the AMPT model gives larger values due to overestimated nonflow effects. As for RHIC [12], anisotropic flows for the most central collisions from the AMPT model are overestimated in comparison with those from the ALICE data, while they are consistent with the ALICE data for mid-central collisions. The reason for this might be due to the constant parton scattering cross section used in the AMPT model for all centralities. Since the temperature of produced partonic matter is higher in central collisions than in mid-central collisions, a smaller strong coupling constant and a larger screening mass [30, 31] should be used in calculating the parton scattering cross section. This is expected to lead to a smaller parton scattering cross section and smaller anisotropic flows for central collisions. We note that once the elliptic flow is fitted, the higher-order flows are automatically consistent with the experimental data. This indicates that the HIJING model, as an initial distribution generator, provides the correct initial spatial anisotropies through the Glauber model calculation.

FIG. 4: (Color online) Two-dimensional dihadron correlation per trigger particle as a function of $\Delta\eta$ and $\Delta\phi$ for $1 < p_T^{\mathrm{assoc}} < 2$ GeV/c and $2 < p_T^{\mathrm{trig}} < 3$ GeV/c for $0-5\%$ most central Pb-Pb collisions at $\sqrt{s_{NN}} = 2.76$ TeV from the string melting AMPT model.

B. Dihadron correlations

As in Ref. [21], we calculate the dihadron correlation according to

$$\frac{1}{N^{\mathrm{trig}}}\frac{d^2 N_{\mathrm{pair}}}{d\Delta\eta d\Delta\phi} = B(0,0) \times \frac{S(\Delta\eta, \Delta\phi)}{B(\Delta\eta, \Delta\phi)}, \qquad (8)$$

where

$$S(\Delta\eta, \Delta\phi) = \frac{1}{N^{\mathrm{trig}}}\frac{d^2 N_{\mathrm{pair}}^{\mathrm{same}}}{d\Delta\eta d\Delta\phi} \qquad (9)$$

is the raw correlation per trigger particle from pairs in same events,

$$B(\Delta\eta, \Delta\phi) = \frac{1}{N^{\mathrm{trig}}}\frac{d^2 N_{\mathrm{pair}}^{\mathrm{mix}}}{d\Delta\eta d\Delta\phi} \qquad (10)$$

is the background correlation per trigger particle from pairs in different events, and $B(\Delta\eta = 0, \Delta\phi = 0)$ is the normalization factor. Eq. (8) is thus similar to Eq. (7) in Sec. II.

In Fig. 4 we show the two-dimensional dihadron correlation per trigger particle from the string melting AMPT model in the $0-5\%$ most central Pb-Pb collisions at $\sqrt{s_{NN}} = 2.76$ TeV for trigger particles and associated particles in the transverse momentum windows $2 < p_T^{\mathrm{trig}} < 3$ GeV/c and $1 < p_T^{\mathrm{assoc}} < 2$ GeV/c, respectively. Similar to the experimental results in Ref. [21], there is a peak at $\Delta\eta = 0$ and a ridge structure extending to $|\Delta\eta| = 4$ at the near side ($\Delta\phi \sim 0$) as well as
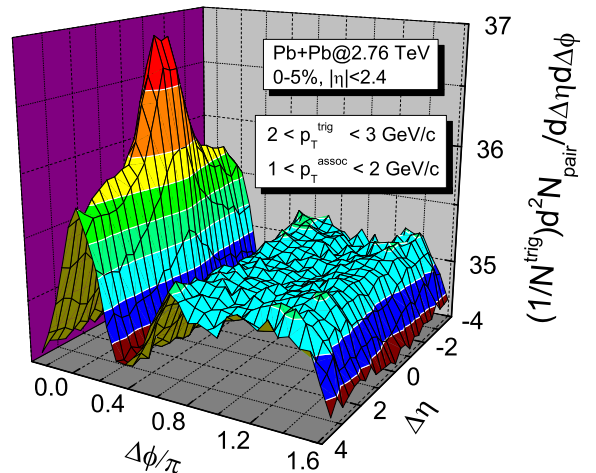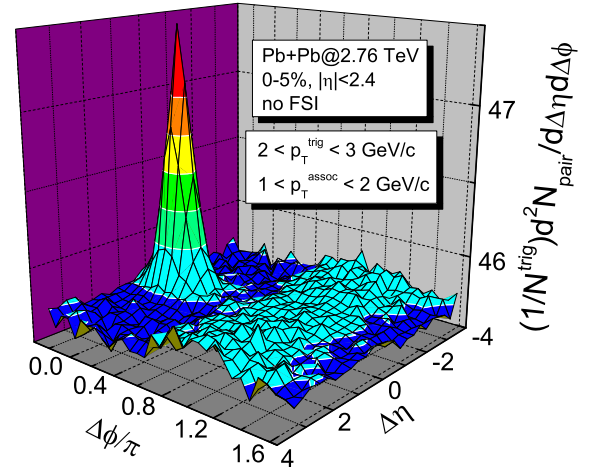

FIG. 5: (Color online) Same as Fig. 4 but without final-state interactions (FSI).

a broad structure at the away side which also extends to $|\Delta\eta| = 4$. The ridge structure was first discovered in Ref. [32]. Many explanations have since been proposed [33–39] until it was recently realized that the ridge was dominated by the anisotropic flows [14, 20, 21] as can be seen from Eq. (7). To illustrate this effect, we re-

peat the calculation by turning off both partonic and hadronic scatterings in the AMPT model, and the results are shown in Fig. 5. It is seen that the near-side ridge now disappears and the away-side broad structure is also largely weakened as both are results of the collective flow that is generated by final-state interactions (FSI). Furthermore, the peak along the $\Delta\eta$ direction is sharper than that in the case with FSI. We note that the wider nonflow contribution in $\Delta\eta$ direction in the case with FSI is related to the early explanations of the ridge structure [33–39].

by taking average of the two-dimensional dihadron correlation over the corresponding $\Delta\eta$ windows [21] as shown in the left and middle columns of Fig. 7 for different transverse momenta of trigger particles. Compared with the short-range correlations, the long-range correlations have much weaker peaks at the near side due to the absence of the nonflow contribution. The strength of the near-side peaks, i.e., the near-side associated yield, decreases with increasing p_T of trigger particles for both short- and long-range correlations, although their heights are similar for short-range correlations. In addition, the strength of away-side correlations decreases with increasing p_T of trigger particles for both short-range and long-range correlations.
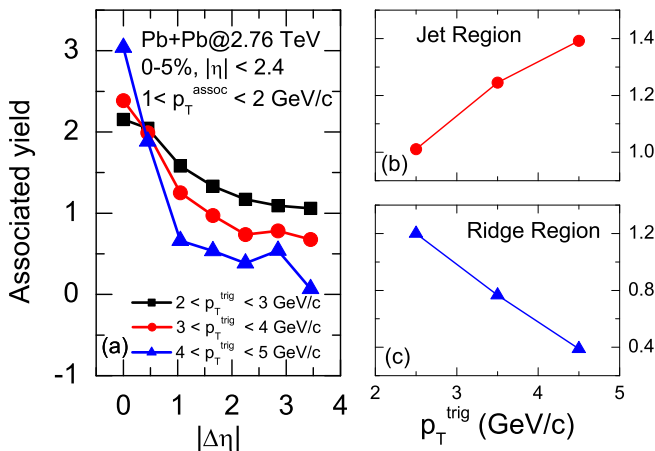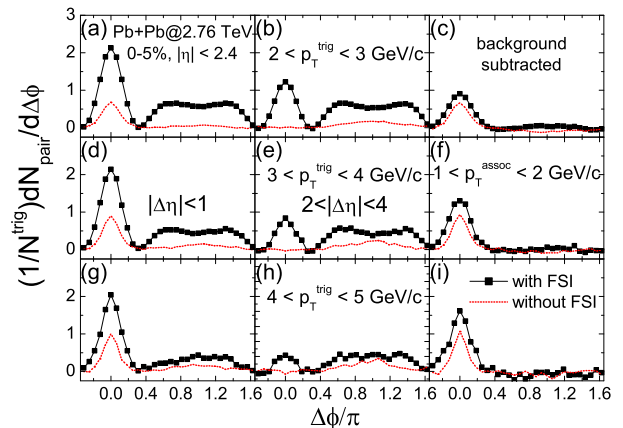

FIG. 6: (Color online) The near-side associated yield as a function of $|\Delta\eta|$ (a) and those as functions of trigger particle transverse momentum in the jet region (b) and the ridge region (c) for $0-5\%$ most central Pb-Pb collisions from the string melting AMPT model.

FIG. 7: (color online) Short-range ($|\Delta\eta| < 1$, (a), (d) and (g)) and long-range ($2 < |\Delta\eta| < 4$, (b), (e) and (h)) dihadron correlations per trigger particle as functions of the azimuthal angular difference $\Delta\phi$ for different transverse momentum windows of trigger particles from $0-5\%$ most central Pb-Pb collisions in the string melting AMPT model with (solid lines) and without (dashed lines) final-state interactions. The difference between the short-range and long-range dihadron azimuthal correlation is shown in panels (c), (f), and (i).

Above results can be quantified by displaying the $|\Delta\eta|$ dependence of the near-side associated yield. Taking the near side as $|\Delta\phi| < \Delta\phi_{\text{ZYAM}}$, with $\Delta\phi_{\text{ZYAM}}$ obtained using the zero-yield-at-minimum (ZYAM) method [40] to fit the dihadron azimuthal correlation by a second-order polynomial in the range $0.5 < \Delta\phi < 1.5$ as in Ref. [21], the results are shown in Fig. 6 (a) for different transverse momentum windows of trigger particles ($2 < p_T^{\text{trig}} < 3$ GeV/c, $3 < p_T^{\text{trig}} < 4$ GeV/c, and $4 < p_T^{\text{trig}} < 5$ GeV/c) but the same transverse momentum window of associated particles ($1 < p_T^{\text{assoc}} < 2$ GeV/c). It shows a similar decreasing trend with increasing $|\Delta\eta|$ as in Ref. [21], and it is broader for the case with lower-p_T trigger particles. The width of the near-side associated yield is related to the broadening of the jet cone affected by the longitudinal flow, and it seems that the jet cone from higher-p_T jets is more focus and less affected by the longitudinal flow.

For the dependence of the near-side associated yield on the trigger particle transverse momentum, we first introduce the short-range ($|\Delta\eta| < 1$) and long-range ($2 < |\Delta\eta| < 4$) dihadron azimuthal angular correlations

Results on the trigger particle transverse momentum dependence of the near-side associated yield in the jet region and the ridge region are shown in Fig. 6 (b) and (c), respectively. In the ridge region, i.e., the long-range correlation ($2 < |\Delta\eta| < 4$), the near-side associated yield decreases with increasing p_T of trigger particles. This is understandable as the near-side ridge is dominated by the collective flow that does not affect much higher-p_T particles. The near-side associated yield in the jet region, which is the difference between the associated yield in the long-range correlation ($2 < |\Delta\eta| < 4$) and the short-range correlation ($|\Delta\eta| < 1$), increases with increasing p_T of trigger particles. This can be again understood as higher-p_T particles are more likely to be accompanied by a larger number of lower-p_T particles because they can fragment into or dump energy to more lower-p_T particles.

All these are qualitatively consistent with the experimental results [21].

Since the dihadron correlation includes contributions from both the anisotropic flows and the medium response to the back-to-back jet pairs produced in initial hard collisions, to isolate the latter effect requires the subtraction of the flow contribution. As discussed in Refs. [14, 20, 21], the long-range dihadron correlation is largely caused by the anisotropic flows and their fluctuations. We can therefore use the long-range dihadron azimuthal correlation shown in the middle column of Fig. 7 as an estimation of the background contribution [14] by neglecting the pseudorapidity dependence of the anisotropic flows and possible non-flow contributions for larger $|\Delta\eta|$. The resulting background-subtracted correlations, i.e., the difference between the short-range correlations and the long-range correlations, are shown in Fig. 7 (c), (f), and (i). It is seen that the resulting away-side correlations are very weak for all cases and this is similar to the results in Ref. [12] obtained using a different method to estimate the background correlations for central collisions. In addition, the near-side correlations in this case are stronger for higher-p_T trigger particles, which can be understood as the stronger medium response to higher-p_T jets. For comparisons, we also show in Fig. 7 by dashed lines the dihadron azimuthal correlations obtained without final-state interactions, which are similar to those from p+p collisions at the same energy. The background-subtracted away-side correlations in this case is similar to that obtained with final-state interactions. The smearing of the away-side jet in heavy ion collisions without final-state interactions or p+p collisions is due to the fairly low p_T of trigger and associated particles considered here, which can lead to an away-side jet with very different pseudorapidity from that of the triggered jet [41] as shown in the middle column of Fig. 7. A peak in the away-side correlations of such collisions would, however, appear if the associated particles have similar momenta as those of the trigger particles or the trigger particles have very high p_T. This is very different from the case where final-state interactions are included. Because of jet quenching as a result of final-state interactions, no peak structure is seen in the away-side correlations unless the trigger particles have extremely high p_T.

IV.   CONCLUSIONS AND DISCUSSIONS

We have studied higher-order anisotropic flows and dihadron correlations in Pb-Pb collisions at $\sqrt{s_{NN}} = 2.76$ TeV within a multiphase transport model with parameters fitted to reproduce the measured multiplicity density of mid-pseudorapidity charged particles in central collisions and their elliptic flow in mid-central collisions in the previous work. We have found that the resulting higher-order anisotropic flows slightly overestimate the experimental data at small centralities but are consistent with them at other centralities. We have obtained the ridge structure along the pseudorapidity direction in the near side of the dihadron correlations, and it disappears when final-state interactions are turned off in our model. We have also studied both the short-range and long-range dihadron azimuthal correlations for different transverse momenta of trigger particles, and they are seen to be quantitatively consistent with experimental results. We have further attempted to determine the background-subtracted short-range dihadron azimuthal correlations by taking the long-range dihadron azimuthal correlations as the background, and they are found to be similar to those obtained previously using a different method.

[1] I. Arsene *et al.* (BRAHMS Collaboration), Nucl. Phys. **A757**, 1 (2005).

[2] K. Adcox *et al.* (PHENIX Collaboration), Nucl. Phys. **A757**, 184 (2005).

[3] B.B. Back *et al.* (PHOBOS Collaboration), Nucl. Phys. **A757**, 28 (2005).

[4] J. Adams *et al.* (STAR Collaboration), Nucl. Phys. **A757**, 102 (2005).

[5] H.C. Song, S.A. Bass, U. Heinz, T. Hirano, and C. Shen, Phys. Rev. Lett. **106**, 192301 (2011).

[6] B. Alver and G. Roland, Phys. Rev. C **81**, 054905 (2010).

[7] P. Sorensen, J. Phys. G **37**, 094011 (2010).

[8] B. Schenke, S. Jeon, and C. Gale, Phys. Rev. Lett. **106**, 042301 (2011).

[9] A. Adare *et al.* (PHENIX Collaboration), arXiv:1105.3928 [nucl-ex].

[10] J. Adams *et al.* (STAR Collaboration), Phys. Rev. Lett. **95**, 152301 (2005).

[11] G.L. Ma and X.N. Wang, Phys. Rev. Lett. 106, 162301 (2011).

[12] J. Xu and C.M. Ko, Phys. Rev. C **83**, 021903 (2011); Phys. ReV. C **84**, 014903 (2011).

[13] H. Agakishiev *et al.* (STAR Collaboration), arXiv:1010.0690 [nucl-ex].

[14] M. Luzum, Phys. Lett. **B696**, 499 (2011).

[15] K. Aamodt *et al.* (ALICE Collaboration), Phys. Rev. Lett. **105**, 252301 (2010).

[16] K. Aamodt *et al.* (ALICE Collaboration), Phys. Rev.

Lett. **105**, 252302 (2010).

[17] K. Aamodt *et al.* (ALICE Collaboration), Phys. Rev. Lett. **106**, 032301 (2011).

[18] K. Aamodt *et al.* (ALICE Collaboration), Phys. Lett. **B696**, 30 (2011).

[19] H. Niemi, G.S. Denicol, P. Huovinen, E. Molnár, and D.H. Rischke, Phys. Rev. Lett. **106**, 212302 (2011).

[20] K. Aamodt *et al.* (ALICE Collaboration), Phys. Rev. Lett. **107**, 032301 (2011).

[21] S. Chatrchyan *et al.* (CMS Collaboration), arXiv:1105.2438 [nucl-ex].

[22] J. Xu and C.M. Ko, Phys. Rev. C **83**, 034904 (2011).

[23] X. N. Wang and M. Gyulassy, Phys. Rev. D **44**, 3501 (1991).

[24] B. Zhang, Comput. Phys. Commun. **109**, 193 (1998).

[25] B. A. Li and C. M. Ko, Phys. Rev. C **52**, 2037 (1995).

[26] Z. W. Lin, C. M. Ko, B. A. Li, B. Zhang, and S. Pal, Phys. Rev. C **72**, 064901 (2005).

[27] G.L. Ma, S. Zhang, Y.G. Ma, X.Z. Cai, J.H. Chen, and C. Zhong, Eur. Phys. J. C **57**, 589 (2008).

[28] S. Wang, Y.Z. Jiang, Y.M. Liu, D. Keane, D. Beavis, S.Y. Chu, S.Y. Fung, M. Vient, C. Hartnack, and H. Stöcker, Phys. Rev. C **44**, 1091 (1991).

[29] N. Borghini, P.M. Dinh and J.Y. Ollitrault, Phys. Rev. C **64**, 054901 (2001).

[30] O. Kaczmarek and F. Zantow, Phys. Rev. D **71**, 114510 (2005).

[31] O. Kaczmarek, F. Karsch, F. Zantow, and P. Petreczky, Phys. Rev. D **70**, 074505 (2004).

[32] J. Adams *et al.* (STAR Collaboration), Phys. Rev. C **73**, 064907 (2006).

[33] N. Armesto, C.A. Salgado, and U.A. Wiedemann, Phys. Rev. Lett. **93**, 242301 (2004).

[34] L.M. Satarov, H. Stöcker, and I.N. Mishustin, Phys. Lett. **B627**, 64 (2005).

[35] C.B. Chiu and R.C. Hwa, Phys. Rev. C **72**, 034903 (2005).

[36] C.Y. Wong, Phys. Rev. C **76**, 054908 (2007).

[37] P. Romatschke, Phys. Rev. C **75**, 014901 (2007).

[38] A. Majumder, B. Müller, and S.A. Bass, Phys. Rev. Lett. **99**, 042301 (2007).

[39] E. Shuryak, Phys. Rev. C **76**, 047901 (2007).

[40] S.S. Adler *et al.* (PHENIX Collaboration), Phys. Rev. Lett. **97**, 052301 (2006).

[41] X.N. Wang, Phys. Rep. **280**, 287 (1997).